Journal of
Micro/Nanolithography,
MEMS, and MOEMS

Nanolithography.SPIEDigitalLibrary.org

Design of electrostatic microcolumn for nanoscale photoemission source in massively parallel electron-beam lithography

Ye Wen
Zhidong Du
Liang Pan

SPIE.

Design of electrostatic microcolumn for nanoscale photoemission source in massively parallel electron-beam lithography

Ye Wen, Zhidong Du, and Liang Pan*
Purdue University, School of Mechanical Engineering, 585 Purdue Mall, West Lafayette, Indiana 47907, United States

Abstract. Microcolumns are widely used for parallel electron-beam lithography because of their compactness and the ability to achieve high spatial resolution. A design of an electrostatic microcolumn for our recent nanoscale photoemission sources is presented. We proposed a compact column structure (as short as several microns in length) for the ease of microcolumn fabrication and lithography operation. We numerically studied the influence of several design parameters on the optical performance such as microcolumn diameter, electrode thickness, beam current, working voltages, and working distance. We also examined the effect of fringing field between adjacent microcolumns during parallel lithography operations. [DOI: 10.1117/1.JMM.14.4.043508]

Keywords: electron-beam lithography; multiple beam direct write; electron optics; microcolumn; maskless lithography.

Paper 15044 received Apr. 14, 2015; accepted for publication Nov. 18, 2015; published online Dec. 18, 2015.

1 Introduction

Electron-beam microcolumns have practical advantages over the traditional columns because of their high resolution and compactness. They are also capable of achieving ultralow landing electron energy for niche applications. Because of their compactness, microcolumns can be arranged into massive arrays for parallel electron-beam lithography. This massive-parallel scheme enables the use of small beam current for each microcolumn to achieve a high total beam current that exceeds the throughput of shaped beam lithography and cell-projection lithography system.[1,2] High-throughput parallel microcolumns have attracted many interests because of their potentials in the applications of electron-beam lithography and imaging. In the past two decades, researchers have developed a variety of miniature electron-beam columns.[3–10] Most of these prototypes utilized the conventional Schottky emitter with high operation temperature (~1800 K), but thermal issues become the biggest obstacle in its development.[11] The use of carbon nanotubes (CNTs) as electron emitters was proposed to replace Schottky emitters; however, there is still no practical approach to fabricate the CNT emitters with the desired consistency and uniformity.[12]

Although there is much research on electron optical systems,[13–19] none of them considered microcolumn designs for nanoscale photocathodes. Laser-excited nanoscale cathodes have been studied by many groups, with source sizes in the range of a few nanometers to several hundreds of nanometers.[20–22] Compared with other cathodes, a nanoscale photocathode can bring many advantages such as high emission brightness, low energy dispersion, low extraction voltage, and easiness of optically switching without using beam blankers. These features allow us to greatly simplify the microcolumn structure and improve the compactness. It is worthwhile to point out that the low initial electron energy and compactness of the microcolumn structure can also allow us to eliminate the use of a limiting aperture and to utilize all of the emitted electrons to obtain reasonably good resolutions. In this paper, we study the possibility of designing an ultracompact electron optical microcolumn with an overall length as short as ~10 μm for a nanoscale photocathode of ~10 nm in size. A conceptual microcolumn has to be designed and optimized. Our optimized designs show the possibility of focusing all of the emitted photoelectrons at nanoscale into a 16-nm spot or smaller in full-width half-maximum (FWHM) at an electron landing energy of 1 keV. Similar structures are sometimes classified as microelectron-guns in many applications. Here, we still named it microcolumn, mainly because it carries more functions than a traditional microgun and can also have beam-deflecting capability. This microcolumn design is compatible with current microfabrication because of its structure simplicity. We also numerically examined microcolumn design for the Coulomb interaction within an individual microcolumn and their fabrication and operation tolerances. It is estimated that an array of 100 × 100 microcolumns can achieve a lithography throughput of about 0.5 wafers per hour (WPH) with a beam current of 1 nA per column.

2 Microcolumn Configuration and Optimization

A traditional electron optical system usually consists of basic components including electrostatic and/or electromagnetic lenses, blankers, and deflectors. For compactness and simplicity considerations, our microcolumns are designed using all electrostatic components.

Figure 1(a) shows the conceptual schematic of our miniaturized electron optics design optimized for a nanoscale photoemission source. The photoemission source is modeled as nanoscale photoelectron-emitting site in a metal film (e.g., gold and chromium) deposited on a transparent substrate

*Address all correspondence to: Liang Pan, E-mail: LiangPan@Purdue.edu

1932-5150/2015/$25.00 © 2015 SPIE

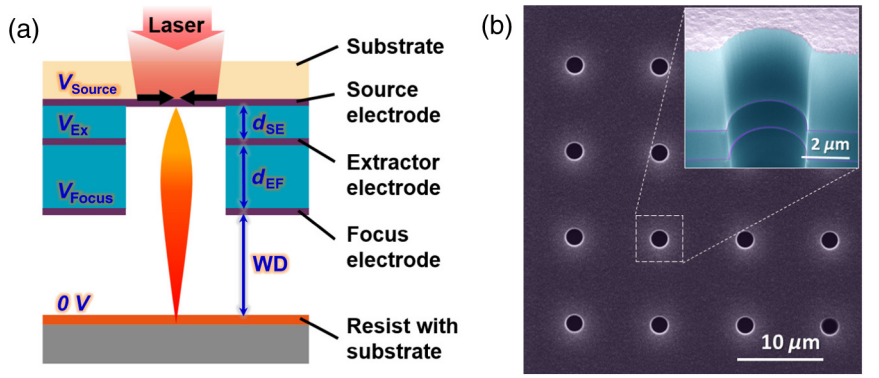

Fig. 1 The electrostatic microcolumn: (a) schematic of the components and parameter names, and (b) an SEM image of a microcolumn array. The inset shows an SEM image of a sectioned microcolumn.

such as quartz. We anticipate that nanoscale photoemission sources are very sensitive to surface contamination, and a vacuum environment better than 10^{-8} Torr is typically required to avoid source degradation and also electrical breakdown. A possible microcolumn array structure is fabricated, shown in Fig. 1(b) as an example, where the inset shows the sectioned microcolumn with layered structures. During the operation of the photoemission source, it is back-illuminated by a laser beam and generates a nanoscale beam of photoelectrons, which will be accelerated and focused into a Gaussian spot by the microcolumn. The electrons can be guided by a deflector [shown in Fig. 3(a)] and rastered over the resist. Compared with the traditional microcolumn, the blanking of the beam can be easily achieved by modulating the incident laser beams; therefore, the electron-beam blanker is not needed, which can significantly reduce the complexities of the fabrication and operation process.

We studied the geometry scaling of a microcolumn design as illustrated in Fig. 1. While keeping the electrode voltages and photocathode size unaffected, all geometric parameters of the microcolumn are presented in a scaling factor using a dimension L_0, where L_0 is the distance between source and extractor. As shown in Fig. 1, the source voltage was fixed at -900 V (V_{Source}), and a bias potential was applied to the extractor electrode of -800 V (V_{Ex}). The focus voltage was optimized, which is approximately -954 V (V_{Focus}), and the resist substrate was grounded (0 V). All electrodes were electrostatic apertures with a diameter of $3L_0$. The distances between the source and the extractor and between the extractor and the focus electrode are L_0 and $2.5L_0$, respectively. The thickness of each electrode was $0.1L_0$. The working distance (WD), which is the distance between the bottom of the focusing electrode and the surface of the resist, was fixed at $5L_0$ in the following discussion unless otherwise specified here. The overall column length was $\sim 9L_0$, which is the total distance from source location to resist surface. The column was designed with a demagnification factor of 0.4. Applied voltages and the structure of electron optics (the aperture diameter, the electrode thickness, and so on) can influence and determine the performance of final probe beam. Thus, it is necessary to evaluate and analyze the influence on the characteristics of the spot size.

Figure 2 shows the resolution dependence for three different scaling factors when varying one design parameter and fixing all others parameters at their optimized values. Influences of different design parameters on the resolution are shown in $L_0 = 1$, 5, and 10 μm, where a constant source size of 10 nm in diameter is maintained when scaling the column size. The obtained results help to examine the manufacturing tolerances and operational parameters of the column designs to meet the desired resolution of 16-nm FWHM beam size. Our simulation indicates that a few percent of variation in dimensions will be acceptable for manufacturing such a microcolumn, which is possible to achieve using state-of-the-art tools. As shown in Fig. 2, the optimized spot size increases as the microcolumn is scaled up. Although scaling up can provide a safer field strength in the insulators, the changes of resolution become more sensitive to the variation of design parameters. The case of $L_0 = 1\,\mu$m is explained here to understand the performance dependence on these parameters. As shown in Figs. 2(a) and 2(b), maintaining the voltage between -804.5 and -795.5 V for extractor and a voltage between -955.6 and -952.4 V for the focusing electrode is necessary to maintain a spot size <16 nm. As shown in Figs. 2(c) and 2(d), a tolerance of 80 nm for the distance between source and extractor and a tolerance of 200 nm for the distance between extractor and focusing electrode are acceptable to maintain the spot size <16 nm. Figures 2(e) and 2(f) suggest that the aperture diameter needs to be kept to be 3 μm with a variation of 40 nm while the thickness of each electrode does not have significant effects on the performance. When fixing the source size at 10 nm, the optimized design for the cases of $L_0 = 5$ and 10 μm is listed in Table 1. During the geometry scaling, the values of optimized parameters scale accordingly but the performance trends to become relatively more sensitive to the same fraction of variations for most of the parameters. These fabrication and operation tolerances are likely affected by the convolution effect between the optical aberrations and the finite source size. In all simulations, the initial energy spread is set to be uniformly distributed from 0.1 to 0.2 eV, and the initial emitting angle with respect to the optical axis is from 0 deg to 90 deg, which are typical for typical photocathodes. In these simulations and the following simulations, we use a commercial electron-optical design software SIMION (version 8.1) to calculate the electrical potential and simulate the electron trajectories. In the case of $L_0 = 1\,\mu$m, the optimized focus voltage was determined to be -954 V at a WD of 5 μm. The electric-field strength of this design is around 190 V/μm for the case of $L_0 = 1\,\mu$m, which is demanding but still safe if high-quality dielectric materials such as fused silica are chosen as the insulators.[23]

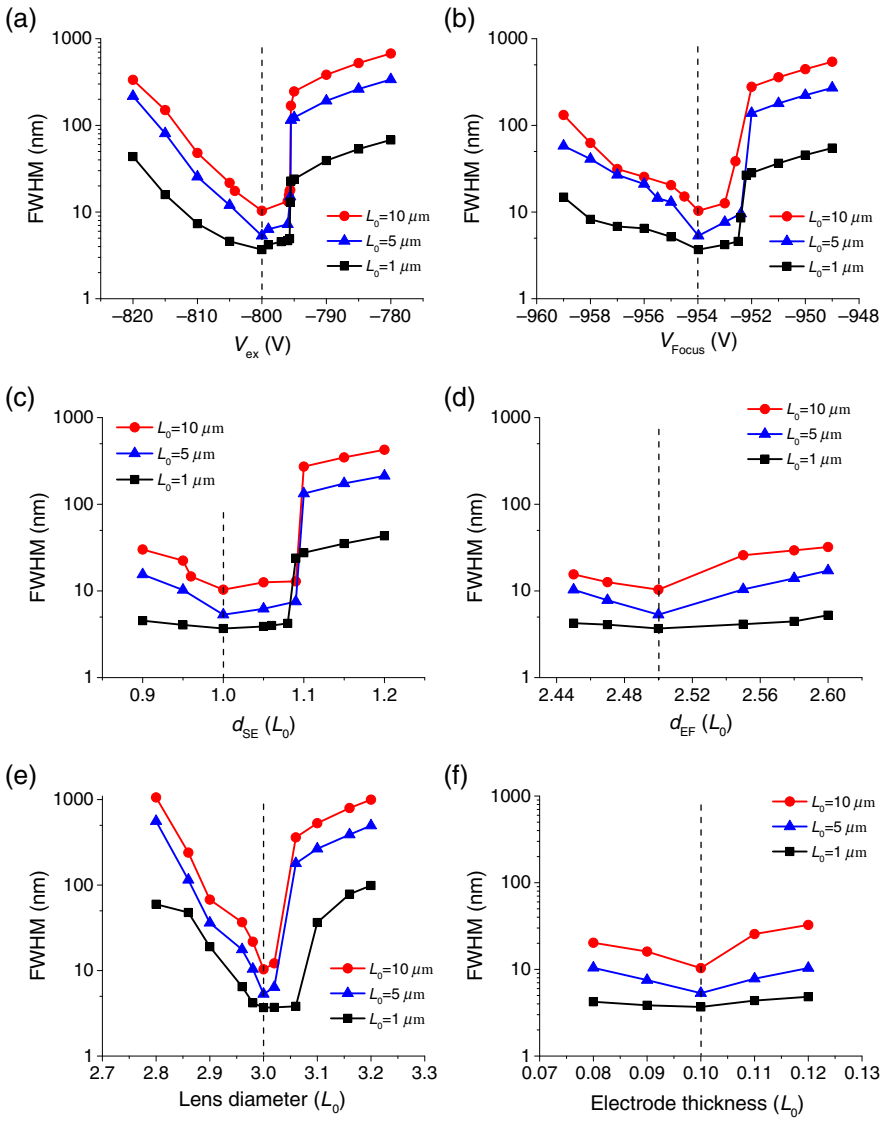

Fig. 2 The scaling capability and the dependence of spot size in FWHM on (a) extraction voltage, (b) focusing voltage, (c) distance between source and extractor, (d) distance between extractor and focusing electrode, (e) aperture diameter, and (f) thickness of each electrode. Dashed lines label the optimized parameter values.

As the column size scales up (for the cases of $L_0 = 5$ and $10\,\mu$m), the field strength will decrease accordingly and a broader range of materials become available.

As shown in Fig. 3(a), a set of quadruple deflectors can be added at $1.5L_0$ away from the focusing electrode and is connected to a center potential of -635 V without causing significant disturbances to the optimized performance and parameters of the microcolumns. The choice of center potential is to maintain original potential distribution after adding the deflector. The diameter of the deflector is chosen to be same as $3L_0$ with a thickness of 200 nm. During its operation, the counter electrodes are offset by the same amount of voltages with opposite polarities. The deflecting performance is analyzed for three scaling factors as shown in Fig. 3. Microcolumn with a larger scaling factor can provide a larger deflection range but causes more beam blur. In the case of $L_0 = 1\,\mu$m, a maximum deflecting voltage of 50 V can be used to obtain a deflection distance of 400 nm while maintaining the beam size of 16 nm. Although the deflectors of the microcolumn array can only cover a fraction of the resist surface, incorporating additional mechanical scanning would allow patterning of a full wafer. To better demonstrate the design guideline and the tolerance, main parameters with tolerances are summarized in Table 1. Although the electrode potentials are relatively unaffected during the scaling, a trade-off between material requirements and manufacturability is obvious judging from these three scaling factors. A smaller column tends to be more robust in the variation of design parameters but requires better electrical insulation and higher vacuum to avoid breakdowns. While a larger column has safer field gradients but requires tighter fabrication tolerances.

3 Performance Analysis and Maximum Operating Current

The optimized beam profiles on the resist surface results using parameters in Table 1 are shown in Fig. 4 under three scaling factors. To achieve practically high-lithography

Table 1 Optimized design parameters.

Design parameters	Case 1 ($L_0 = 1\,\mu$m)	Case 2 ($L_0 = 5\,\mu$m)	Case 3 ($L_0 = 10\,\mu$m)
Initial energy (eV)	0.1 to 0.2	0.1 to 0.2	0.1 to 0.2
Launch angle of electron source (deg)	0 to 90	0 to 90	0 to 90
Voltage of source (V_{Source}) (V) (fixed)	−900	−900	−900
Voltage of extractor (V_{Ex}) (V)	-800 ± 4.5	-800 ± 4.4	-800 ± 4.2
Voltage of focus electrode (V_{Focus}) (V)	-954 ± 1.6	-954 ± 1.5	-954 ± 0.5
Voltage of wafer (V) (fixed)	0	0	0
Source and extractor spacing (d_{SE}) (μm)	1 ± 0.08	5 ± 0.45	10 ± 0.40
Extractor and focus lens spacing (d_{EF}) (μm)	2.5 ± 0.2	12.5 ± 0.1	25 ± 0.3
Lens diameter (μm)	3 ± 0.04	15 ± 0.1	30 ± 0.2
Thickness of each electrode (nm)	100	500	1000

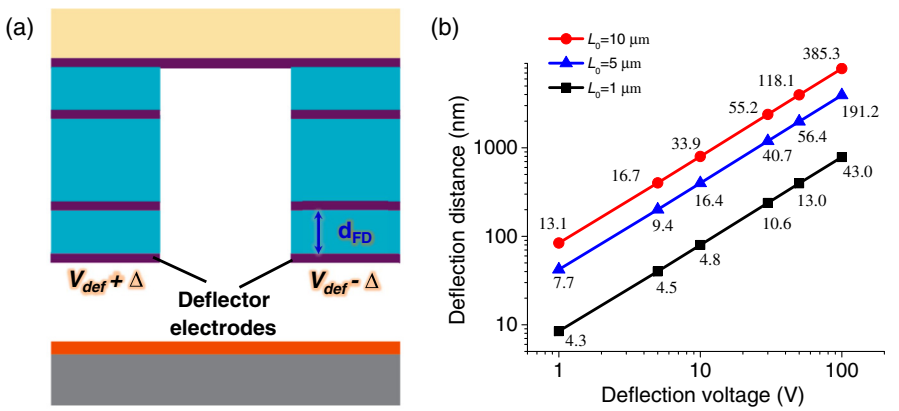

Fig. 3 (a) Cross-section view of the quadruple deflector, and (b) beam displacement versus change of deflection voltage. The spot sizes are labeled in the figure in FWHM.

throughput, large landing beam currents are desired. However, extremely large beam current will cause noticeable electron–electron interaction (Coulomb interaction). The image blur due to Coulomb interaction increases with beam current, optical column length, and demagnification but decreases with convergence angle, source size, and acceleration voltage.[24] The Coulomb interaction can be negligible by distributing the total beam current among microcolumn array, reducing microcolumn length and source size and increasing the acceleration voltage and so on. In Fig. 5, all optimized parameters in Table 1 are applied and the figure shows the effect of beam blur induced by Coulomb interaction using a 10-nm-diameter source. It is shown that the microcolumn can operate at a large beam current reaching tens of nanoamperes without noticeable beam blur for $L_0 = 1\,\mu$m and the current limit reduces to several nanoamperes and hundreds of picoamperes for $L_0 = 5$ and $10\,\mu$m, respectively. The source voltage of −900 V was fixed in investigating the intercolumn interaction.

4 Microcolumn Fabrication and Operational Tolerances

The off-axis aberrations and the depth of focus (DOF) in three scaling factors are numerically evaluated for the fabrication and operational tolerances of the microcolumn. In Figs. 6(a)–6(c), the electrons are emitted from an off-axis distance (x) in the source plane, the focus distributions are plotted at the targeted plane for the center offset (y), and the FWHM is shown as error bars. The seven sources are simulated with 5-nm spacing. At the image plane, the deviation was plotted as the function of source position. Figure 6(a) shows that as the source offset increases, the beam spot shifts according to the magnification factor of the microcolumn. An offset of less than 30 nm can keep the spot size <16 nm in all three scales. This alignment accuracy of 30 nm is achievable using existing microfabrication facilities to accurately align the photocathode without a significant loss in resolution. In practice, it may not be trivial to achieve an alignment accuracy of 30 nm within all columns. The

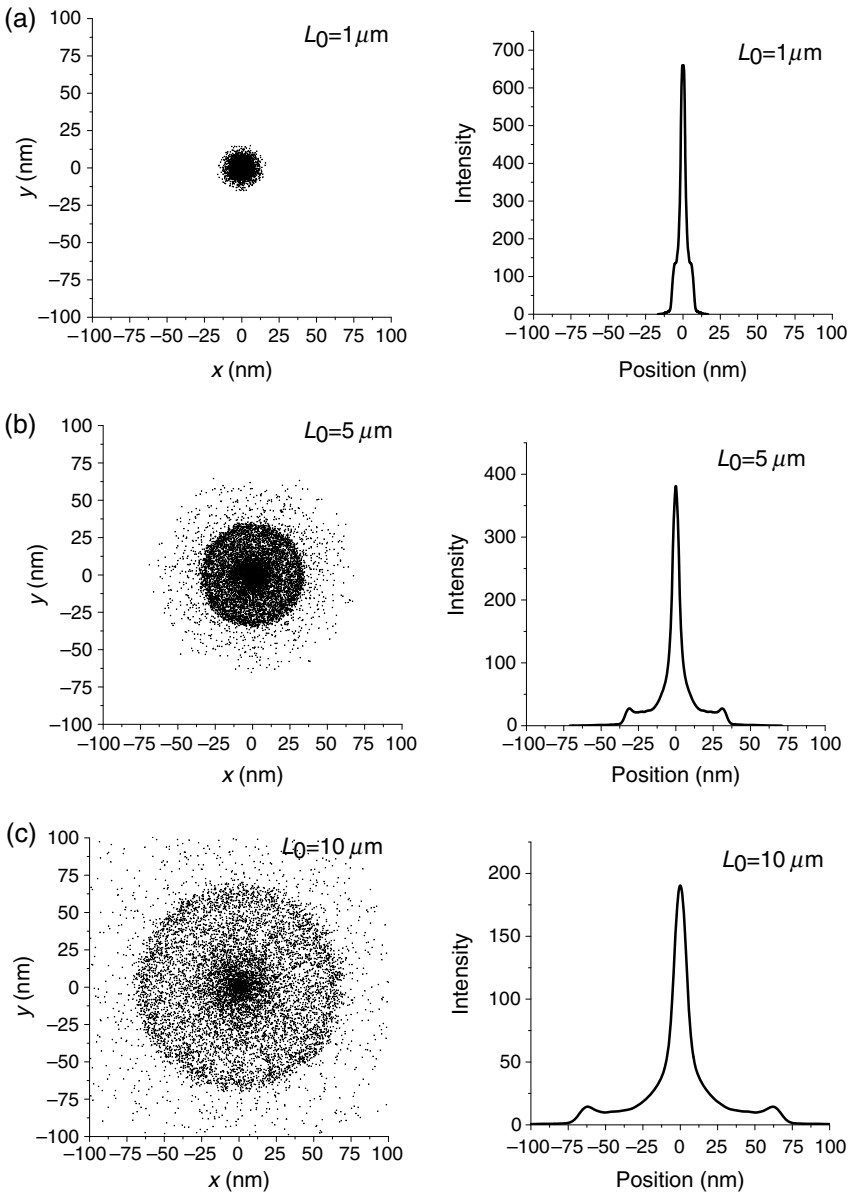

Fig. 4 Spot diagram of the microcolumn with 10-nm-diameter source. The size in full-width half-maximum is (a) 3.69 nm for $L_0 = 1\,\mu$m, (b) 5.32 nm for $L_0 = 5\,\mu$m, and (c) 10.34 nm for $L_0 = 10\,\mu$m.

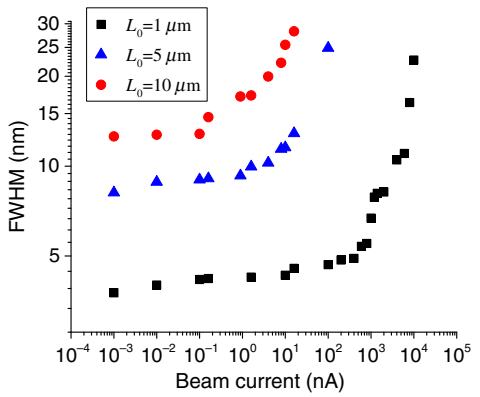

Fig. 5 Electron–electron interaction simulation of single column. The spot size was plotted as a function of the beam current. The microcolumn is capable of keeping the spot size variation <10% over a large current range.

influence of DOF on the probe beam diameter is shown in Fig. 6(b). Our design was optimized at WD of 5 μm. Figure 6(d) indicates that a WD variation between $4.85L_0$ and $5.2L_0$ is acceptable which still maintains a spot size <16 nm but a larger variation can cause severe blur. Obviously the resolution performance is more sensitive to WD for a larger scale which could lead to challenges in the lithography operation.

5 Intermicrocolumn Interaction

Although electron-beam direct writings using microcolumns provide a superb lithography resolution, the low throughput is the main obstacle in their applications. Using a massive number of microcolumns in parallel can largely increase throughput. Many efforts have been devoted to developing microcolumn arrays and multiple miniature columns to improve the throughput.[25–31] The analysis indicates that larger number of microcolumns can provide the potential

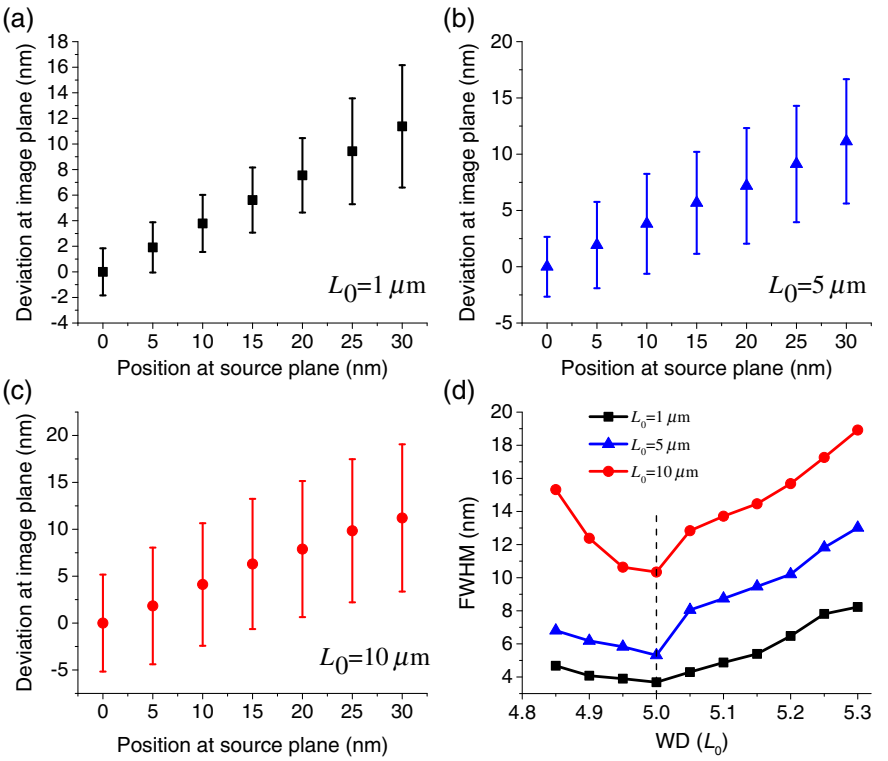

Fig. 6 Performance of the microcolumn under three scaling factors for (a)–(c) off-axis source alignment and (d) working distance.

opportunity to increase throughput. However, the number of microcolumns is limited by several factors. The major one is space charge effect (Coulomb interactions); however, this can be neglected in our design if the operating beam current is well below 100 nA for each microcolumn. The second is the beam aberration and drift caused by the fringing fields of the adjacent apertures. It is important to ensure that the microcolumns are positioned far enough to minimize the intermicrocolumn interactions.

To evaluate a reasonable footprint size of a 100×100 microcolumn array, we analyzed the interaction between two microcolumns with $L_0 = 1\,\mu$m at a spacing in the range of 4 to 13 μm. We constructed two microcolumns in three-dimensional (3-D) model and varied their center-to-center distance while keeping their distances from the boundaries of the simulation domain to be large enough (10 μm and larger) to minimize the boundary influence. Figure 7 shows the drift of the beam center caused by the fringing field from adjacent microcolumn for the case of $L_0 = 1\,\mu$m. The beam drift reduces rapidly when their aperture center-to-center distance increases in the range of 4 to 8 μm. As the distance further increases, the discretization errors from the 3-D model will start to take over, leading to noise floor of a few nanometers. The trend shown in Fig. 7 indicates that the fringing field from adjacent microcolumn can be neglected when their aperture center-to-center distance is larger than 12 μm. Simulations for the cases of $L_0 = 5$ and 10 μm are not performed due to compute-intensive nature of the 3-D models. We expect the beam drift to scale linearly with respect to L_0, which would require further scaling up the center-to-center distance to a value even higher than $12L_0$ in order to the same magnitude of beam drift.

Because of the compactness of the microcolumns, it is possible to scale up the total number of microcolumns to achieve an adequate throughput in lithography. The overall lithography throughput depends on the number of microcolumns and the current of each column. The writing time T can be evaluated as $T = (A \cdot S)/(N \cdot I)$, where A is the wafer surface area, S is the resist sensitivity, N is the number of microcolumns in use, and I is the beam current of each microcolumn. If we assume microcolumn array needs to scan over the whole area (i.e., 100% surface coverage) and an emission current of 1 nA is achievable for each photocathode, a throughput of 0.5 WPH on 12-in. wafers is

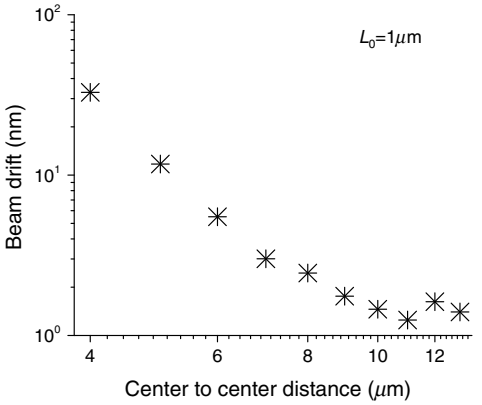

Fig. 7 Dual-column interaction with different aperture center-to-center distances for $L_0 = 1\,\mu$m. It shows that a minimum spacing of 12 μm can safely avoid the field distortion effect from the adjacent microcolumns.

achievable with the resist sensitivity of $100\,\mu C/cm^2$ using 10,000 microcolumns.

Limited by the compute-intensive nature of the 3-D model, above intermicrocolumn simulation neglects the influence of the deflectors. In addition to the influence of adjacent deflectors, a thorough investigation of the intermicrocolumn interaction is yet to be done with considerations of more factors such as distortion of spot shape and size.

6 Summary

We proposed an electrostatic microcolumn to use with a new nanoscale photoemission source. The microcolumn design was optimized for a high-resolution 10-nm source with low-beam landing energy (~1 keV). Considering the fabrication and operation processes, we analyzed the scaling capabilities, tolerances of microcolumn parameters (including bore diameter, electrode thickness, off-center alignment, WD, electrode voltages, and so on) based on different scales. We also evaluated maximum allowable operating beam current by studying Coulomb interactions and determined the required spacing between microcolumns. This microcolumn with a novel nanoscale photoemission source is suitable for parallel multiple columns implementation.

Acknowledgments

Support to this work by the National Science Foundation (Grant No. CMMI-1405078) was gratefully acknowledged. The authors were grateful to Professor Xianfan Xu from the School of Mechanical Engineering at Purdue University for his helpful discussions.

References

1. H. C. Pfeiffer et al., "EL-4, a new generation electron-beam lithography system," *J. Vac. Sci. Technol. B* **11**(6), 2332–2341 (1993).
2. Y. Nakayama et al., "Electron-beam cell projection lithography: a new high-throughput electron-beam direct-writing technology using a specially tailored Si aperture," *J. Vac. Sci. Technol. B* **8**(6), 1836–1840 (1990).
3. A. Cerezo and M. Miller, "Einzel lenses in atom probe designs," *Surf. Sci.* **246**(1), 450–456 (1991).
4. M. Despont et al., "Microfabrication of lenses of a miniaturized electron column," *Microelectron. Eng.* **27**(1), 467–470 (1995).
5. T. H. P. Chang, D. P. Kern, and L. P. Muray, "Microminiaturization of electron optical systems," *J. Vac. Sci. Technol. B* **8**(6), 1698–1705 (1990).
6. Y. C. Kim et al., "Inspection method for contact/via-holes using a low-energy electron microcolumn," *J. Vac. Sci. Technol. B* **27**(6), 3208–3212 (2009).
7. E. Kratschmer et al., "Experimental evaluation of a 20×20 mm footprint microcolumn," *J. Vac. Sci. Technol. B* **14**(6), 3792–3796 (1996).
8. L. P. Muray et al., "Performance measurements of a 1-keV electron-beam microcolumn," *J. Vac. Sci. Technol. B* **10**(6), 2749–2753 (1992).
9. T. S. Oh et al., "Inspection of open defects in a thin film transistor-liquid crystal display panel by using a low-energy electron microcolumn," *J. Vac. Sci. Technol. B* **28**(6), C6C69 (2010).
10. R. Saini et al., "Assembled microelectromechanical system microcolumns for miniature scanning electron microscopies," *J. Vac. Sci. Technol. B* **24**(2), 813–817 (2006).
11. R. Saini et al., "Assembled micro-electromechanical-systems microcolumn from a single layer silicon process," *J. Vac. Sci. Technol. B* **22**(6), 3168–3173 (2004).
12. N. de Jonge et al., "Optical performance of carbon-nanotube electron sources," *Phys. Rev. Lett.* **94**(18), 186807 (2005).
13. C.-D. Bubeck et al., "Miniature electrostatic lens for generation of a low-voltage high current electron probe," *Nucl. Instrum. Methods Phys. Res., Sect. A* **427**(1), 104–108 (1999).
14. S.-Y. Chen et al., "Manufacturability analysis of a micro-electro-mechanical systems-based electron-optical system design for direct-write lithography," *Jpn. J. Appl. Phys.* **49**(6), 06GE05 (2010).
15. Y. C. Kim et al., "Effect of the einzel lens structure in microcolumn," *Jpn. J. Appl. Phys.* **43**(6B), 3728–3730 (2004).
16. M. Mankos, "Electron optics for dual-beam low energy electron microscopy," *Nucl. Instrum. Methods Phys. Res., Sect. A* **645**(1), 35–40 (2011).
17. T.-S. Oh et al., "Improved design of 5 nm class electron optical microcolumn for manufacturing convenience and its characteristics," *J. Vac. Sci. Technol. A* **31**(6), 061601 (2013).
18. T. S. Oh et al., "Design of an ultra-miniaturized electron optical microcolumn with sub-5 nm very high resolution," *Ultramicroscopy* **136**, 171–175 (2014).
19. E. D. Liu et al., "Analysis of multibeam's scalable column for complementary e-beam lithography (CEBL)," *Proc. SPIE* **8323**, 83231X (2012).
20. A. W. Baum et al., "Semiconductor on glass photocathodes for high throughput maskless electron beam lithography," *J. Vac. Sci. Technol. B* **15**(6), 2707–2712 (1997).
21. P. Hommelhoff et al., "Field emission tip as a nanometer source of free electron femtosecond pulses," *Phys. Rev. Lett.* **96**(7), 077401 (2006).
22. C. Ropers et al., "Localized multiphoton emission of femtosecond electron pulses from metal nanotips," *Phys. Rev. Lett.* **98**(4), 043907 (2007).
23. L. Berger, "Dielectric strength of insulating materials," in *CRC Handbook of Chemistry and Physics*, 96th ed., (2015–2016).http://www.hbcpnetbase.com
24. H. C. Pfeiffer, "New prospects for electron beams as tools for semiconductor lithography," *Proc. SPIE* **7378**, 737802 (2009).
25. E. Slot et al., "MAPPER: high-throughput maskless lithography," *Proc. SPIE* **6921**, 69211P (2008).
26. H. Yasuda, A. Yamada, and M. Yamabe, "Multi column cell (MCC) e-beam exposure system for mask writing," *Proc. SPIE* **7028**, 70280B (2008).
27. M. Mankos et al., "Multisource optimization of a column for electron lithography," *J. Vac. Sci. Technol. B* **18**(6), 3010–3016 (2000).
28. P. Petric et al., "REBL: a novel approach to high speed maskless electron beam direct write lithography," *J. Vac. Sci. Technol. B* **27**(1), 161–166 (2009).
29. F. M. Schellenberg et al., "PML2: the maskless multibeam solution for the 22 nm node and beyond," *Proc. SPIE* **7271**, 72710N (2009).
30. H. Yasuda et al., "Multiaxis and multibeam technology for high throughput maskless E-beam lithography," *J. Vac. Sci. Technol. B* **30**(6), 06FC01 (2012).
31. E. Yin et al., "Electron optical column for a multicolumn, multibeam direct-write electron beam lithography system," *J. Vac. Sci. Technol. B* **18**(6), 3126–3131 (2000).

Ye Wen received his MS degree in mechanical engineering from the School of Mechanical Engineering, Purdue University, West Lafayette, Indiana, USA, in 2015. His work focuses on design of microscale electron optics system in electron-beam lithography.

Zhidong Du is a PhD student at the School of Mechanical Engineering, Purdue University, West Lafayette, Indiana. His research focuses on nanoscale optics and heat transfer applications in electron-beam lithography.

Liang Pan is an assistant professor at the School of Mechanical Engineering, Purdue University, West Lafayette, Indiana. His research focuses on the fundamentals of micro- and nanoscale engineering for applications such as lithography, imaging, and data storage.